Radiophysics and Quantum Electronics, Vol. 42, No. 7, 1999

SPATIO-TEMPORAL DEVELOPMENT OF THE FILAMENTS DUE TO THE THERMAL SELF-FOCUSING INSTABILITY NEAR THE CRITICAL SURFACE IN IONOSPHERIC PLASMAS

N. A. Gondarenko,[1] P. N. Guzdar,[1] G. M. Milikh,[2]
A. S. Sharma,[2] K. Papadopoulos,[2]
and S. L. Ossakow[3]

UDC 537.868

We study fully nonlinear spatio-temporal development of the thermal self-focusing instability of high-power radio waves near the critical surface of the ionosphere. These simulations improve on our earlier work by including an evolution equation for the density instead of using the assumption of constant pressure to determine the perturbed density connected with the known temperature perturbation. Using our two-dimensional nonlinear code we analyze the time scale and associated velocity for the development of the field-aligned irregularities as they spread from the critical surface both in the underdense as well as the overdense regions. The scaling of this velocity as a function of the radiated power of the heater electromagnetic wave (ERP) is determined. We also study the characteristic size of the self-focused filament as a function of ERP. Finally, the spectrum of the density and temperature fluctuations as well as modifications in the equilibrium values of these parameters for different values of ERP are presented.

1. INTRODUCTION

The ionospheric modification experiments using radio frequence (RF) heater facilities at Arecibo, Platteville, Alaska, the "Sura" facility in Russia, and the facility of Tromso, Norway, provide a rich variety of results related to the spatial and temporal structures in the ionospheric medium, the scattered electromagnetic signals, and electron energization [1–8]. These experiments have shown that increase in high frequence (HF) power results in the creation of irregularities some of which can be attributed to the thermal self-focusing instability [1, 9–14]. Observations made with ionosondes [15], scintillation studies [16–19], radar scattering [20, 21], in-situ satellite measurements [22], optical emissions [23], dynasonde HF radar [24], and in-situ rocket measurements [25] have revealed the excitation of irregularities in the medium during the RF heating experiments, which have been attributed to the self-focusing instability (SFI). There are other nonlinear processes that can occur in the vicinity of the critical surface, namely the oscillating two-stream instability or the modulational instability, which leads to strong Langmuir turbulence [26] and the parametric decay instability [27, 28] both driven by the ponderomotive force. These processes generate short scale length (less than or of the order of meters) fluctuations, which occur in the unconditioned ionospheric plasma in the very early phase (less than tens of milliseconds). Our focus is on processes that occur on the longer heating timescales (from 100 ms to few seconds) and generate irregularity scales of tens of meters to kilometers.

---

[1] Institute for Plasma Research, University of Maryland, College Park, MD 20742, USA; [2] Department of Astronomy, University of Maryland, College Park, MD 20742, USA; [3] Plasma Physics Division, Naval Research Laboratory, Washington, DC 20375, USA. Translated from Izvestiya Vysshikh Uchebnykh Zavedenii, Radiofizika, Vol. 42, No. 7, pp. 670–681, July 1999. Original article submitted January 11, 1999.

Bernhardt and Duncan [13] have carried out two-dimensional (2D) numerical simulations of the self-focusing instability in the underdense plasma including a detailed inhomogeneous model of the ionosphere as well as the magnetic field of the Earth. They included an initial sinusoidal perturbation of the density in the case of underdense plasma when the pump wave was represented by a plane wave. This density perturbation leads to the linear growth of the SFI at the same wavelength. Their results showed that the initial pattern evolved into a distorted pattern (due to nonlinear effects) with smaller-scale sizes. The fundamental limitation of this study is that they focus on the underdense plasma, where there is no clear observational evidence of structuring. Few of the theoretical studies have extrapolated the results to the critical density and overdense region, where there is a preponderance of evidence for a broad spectrum of scale sizes, from kilometers to tens of meters. Cragin et al. [10], Gurevich [11], and Das and Fejer [29] have developed theories for the linear stability of the thermal SFI in the vicinity of the critical surface and have found that it is an absolute instability, unlike the underdense case. Gurevich et al. [30] have recently developed a nonlinear theory for a single thermal filament. In their work they first excite upper-hybrid waves, with the high-powered heater, in the region between the upper hybrid resonance and plasma resonance and study the nonlinear thermal filamentation of the upper-hybrid wave. In this paper the focus is on studying the thermal self-focusing and filamentation of the electromagnetic heater wave (without converting it into the upper hybrid mode) near the critical surface. A two-dimensional code to study the nonlinear thermal self-focusing instability in the vicinity of the critical surface of the ionosphere [31] was developed. In this investigation we had a set of nonlinear equations coupling the electromagnetic heater wave with the temperature equation for the electrons. The density perturbations associated with this instability was evaluated by assuming the plasma pressure to be constant and computing the perturbed density knowing the perturbed temperature. This study was the first to address the full nonlinear time-development of the instability starting at the critical surface and developing filamentary structures along the field-line. In the present work we have improved on the modelling by introducing a separate equation for the density evolution and studied in detail characteristics of the heater induced irregularities. Our results are also compared to some recent observations.

The paper is organized as follows. In Sec. 2 the basic nonlinear system of equations for the thermal filamentation in the region of the critical surface are introduced. Various numerical considerations which play a role in determining our choice of the computational box are discussed in Sec. 3. In this section we also discuss the issues related to the boundary conditions. This is followed by a presentation of the results obtained from the solution of these equations in Sec. 4. We compare these results to some observations at the "Sura" and Tromso heating facilities. Finally a brief discussion of our main results is summarized in Sec. 5.

2. BASIC EQUATIONS

We consider the basic geometry for the wave propagation and the orientation of the magnetic field B_0 in the high-latitude ionopshere. The wave propagates vertically upward along the magnetic field in the z direction. The plasma density is assumed to increase as a function of z. The basic equations are [11]

$$\left[c^2\nabla^2 - \frac{\omega\omega_{\rm pe}^2(z_{\rm c})}{\omega + i\nu_{\rm e} \mp \Omega_{\rm e}}\left(\frac{n(z) - n_0(z_{\rm c})}{n_0(z_{\rm c})}\right)\right] E_{0\pm} = 0, \tag{1}$$

$$\frac{\partial T}{\partial t} = \frac{\partial}{\partial z}\left(\chi_\parallel \frac{\partial T}{\partial z}\right) + Q - L, \tag{2}$$

$$\frac{\partial n}{\partial t} = \frac{\partial}{\partial z}\left(D_\parallel \frac{\partial n}{\partial z}\right) + \frac{\partial}{\partial z}\left(D_\parallel^T \frac{\partial T}{\partial z}\right) + q - \beta n N. \tag{3}$$

The first equation is the wave equation for the extraordinary (X) E_{0+} mode or the ordinary (O) mode E_{0-} with the heater wave frequency ω. Here $\omega_{\rm pe} = \sqrt{4\pi e^2 n/m_{\rm e}}$ is the electron plasma frequency, e

is the elementary charge, m_e is the electron mass, n_0 and n are equilibrium and perturbed electron density, respectively, $\Omega_e = eB_0/m_e c$ is the electron cyclotron frequency, c is the velocity of light, and $\nu_e = \nu_{ei} + \nu_{en}$ is the sum of the electron-ion and electron-neutral collision frequencies. The surface $z = z_c$ is the critical surface where the local plasma frequency $\omega_{pe}(z_c)$ matches the frequency ω. The second equation is the equation for the electron temperature T, where $\chi_{\|}$ is the parallel thermal conduction coefficient, Q is the time-averaged ohmic heating by the wave defined as

$$Q = \frac{e^2 E_{0\pm}^2 \nu_e}{3m_e[(\omega \mp \Omega_e)^2 + \nu_e^2]}, \tag{4}$$

L is the sum of the losses due to Coulomb collisions, electron-neutral collisions excitation of fine-structure, rotational excitation, and vibrational excitations [32]. Equation (3) for the evolution of the density is the major new addition to our earlier model [31]. Also, $D_{\|}$ and $D_{\|}^T$ are the diffusion and the thermal diffusion, respectively, q is the ionization source, $\beta n N$ is the loss due to recombination in the F-layer, where it is determined by the conversion rate β of atomic O^+ into molecular NO^+, and N is the number density for the molecular nitrogen. If the parallel transport dominates the density evolution, the perturbed density evolves to keep the pressure constant along the magnetic field lines.

We now introduce the following normalizations to derive a set of dimensionless equations. In the present study we will consider a linear density profile in the z (vertical) direction, with a characteristic scale-length L_n. We normalize the spatially independent variables x and z to the Airy length $z_0 = (c^2 L_n/\omega^2)^{1/3}$, and time t to $t_0 = (2\omega z_0^2/c^2)$. We define $T = T_b + T_1$, where T_1 is perturbed temperature related to the change in electron temperature T from the background ion temperature T_b. The perturbed temperature $T_1/T_b = \theta/\alpha$. Then we get that the new perturbed temperature $\theta = \alpha(T - T_b)/T_b$, with $\alpha = \omega^2 z_0^2/c^2$. The density is normalized to $n_0(z_c)$ and the wave amplitude is redefined as the jitter velocity $eE_{0\pm}/m\omega$, which is normalized to $\sqrt{(6/\alpha)}c_s$. Here c_s is the ion sound velocity computed with the electron temperature.

3. NUMERICAL PRELIMINARIES

We first choose a typical set of plasma parameters which are needed to evaluate the various dimensionless parameters derived in Sec. 2. We choose high-latitude F-region parameters. The incident wave is assumed to have the frequency $f_0 = 5$ MHz. The magnetic field equals $B_0 = 0.5$ G, and the electron temperature, $T = 0.1$ eV. For this particular choice of the parameters the value $\alpha = 561$. Since we consider propagation along the magnetic field, the only difference between the O mode and the X mode is the position of the reflection point in z and a difference in the heating Q. The position of the reflection height z_c is obtained from the relationship $\omega_{pe}^2(z_c) = \omega^2(1 \mp \Omega_e/\omega)$. Here $\mp$ refers to the X mode and O mode, respectively. In the F region, the wave frequency is about five times larger than the gyro-frequency within our present model. Thus, there is no significant difference in heating characteristics between the O mode and X mode, since the heater wave behaves as if the plasma is unmagnetized. Of course this is only true for the case of propagation along the magnetic field. This is a limitation of the present work. In future work we will address propagation at a finite angle to the magnetic field and finite angle between the direction of the density gradient and the magnetic field. The differences between O mode and X mode heating will be more significant due to differences in their mode conversion properties [33]. The plasma is assumed to have a linear density profile with the scale length $L_n = 100$ km. We will hold these parameters as constants for the runs we discuss and will vary the intensity of the incident radiation.

We now discuss various issues related to our numerical code. The number of grid points in the x direction $N_x = 64$, while the number of grid points in the z direction $N_z = 256$. The next important aspect of the simulations to discuss are the boundary conditions. At the lower boundary, $z = 0$, we specify E_0 and at the top boundary, $z = L_z$, the wave amplitude is chosen to be zero. This is because beyond the critical surface at the center of the simulation box, the wave is evanescent. For the temperature and the density, the boundary conditions in z are that the derivative of each of these quantities with respect to z

be zero. This is because the parallel diffusion and thermal conduction transport the energy away from the region of heating and allow it to escape through the boundary. In reality the boundary condition should be the continuity of the heat and particle fluxes along the field line. However, since both transport coefficients are very large, constant temperature and perturbed density tend to be established along the fieldline. The equilibrium density is maintained by the source. Thus at the boundary points we set the perturbed density and the temperature equal to that at the nearest point within the computation box. For the lowest-order finite-difference scheme this is equivalent to parallel gradient being set equal to zero. In the x direction, transverse to the magnetic field, for all the three dependent variables we use periodic boundary conditions. The numerical scheme used is a finite-difference leap-frog scheme for evolving the density and temperature and a pseudo-spectral relaxation scheme for the wave equation [31].

The choice of the size of the box in the two directions needs to be addressed in some detail. The characteristic size in the x direction should be the basic size of the heating region, which is typically about $30-50$ km. Because of the self-focusing instability we anticipate the shortest scale lengths to be of the order of 10 to 100 meters. This would require a very large number (at least 10^4) of grid points in this direction to resolve the longest as well as the shortest scale sizes in the problem. Thus due to this computational constraint we choose the size of the computation box in the x direction to be of the order of the 1 km. This will allow us to resolve the shortest scale lengths we expect to obtain in the nonlinear phase. For the present-day intensities, even scale lengths of the order of a kilometer are linearly unstable. These short scale lengths, though linearly stable, are generated by the nonlinear "collapse" due to the self-focusing instability. In the recent work [19], electron density irregularitities in the F region, excited by the European Incoherent Scatter (EISCAT) high-power facility at Tromso, Norway, and observed by scintillations of the 250 MHz satellite signals, show that the spectra are in the range of kilometers to tens of meters. Since the power-density used in our studies is in the range used at Tromso, the choice of the scale-lengths is relevant to these observations.

In the z direction the shortest scale-size is the Airy length. For the parameters chosen, this is typically about 180 m. For $N_z = 256$, the box size in the z direction is 9 km. Finally, our initial conditions are the following: the temperature is uniform in the box, the density has linear variation in z and the wave is launched from the lower boundary. We introduce a 1.0% density perturbation with eight harmonics of the basic periodic length in x and the same amplitude. This initial perturbation is localized in a small region in z around the critical surface to seed the instability.

4. NUMERICAL RESULTS

Let us first discuss the results for the heater wave intensity of 0.3 mW/m^2. Figure 1 shows the normalized wave amplitude and the normalized perturbed temperature and density contours at three different instants of time. The heater wave reflected at the critical surface at $L_z/2$ three milliseconds after its launching from $z = 0$. The wave amplitude is basically an Airy-like pattern (Fig. 1a). The Airy swelling increases the amplitude at the critical surface. We also see that the longest wavelength mode (in x) grows localized in z in the first Airy peak near the reflection height. In this very early phase, the temperature in the underdense plasma has increased by a fraction of a percent. However, at the reflection height, the localized region of the wave intensity has led to localized heating of the plasma as seen on the temperature contours of Fig. 1b. Another interesting feature that emerges from the comparison of the localized hot spot for the wave and the temperature is that the extent of the temperature hot spot along the z direction is larger than the Airy length, the spatial extent of the heater wave enhanced region. This is due to the parallel heat transport along the field lines (in the z direction) which diffuses the heat. Since the perturbed temperature is about 0.27%, the associated changes in the density are not apparent on the density contours in Fig. 1c. Both the normalized wave amplitude and normalized perturbed temperature are large, because of the large value of the parameter α, in the normalization.

At a later time $t = 0.33$ s, we observe an interesting phenomenon. As the single hot spot diffuses both above and below the original reflection height, in the underdense region the wave gets redirected and spawns

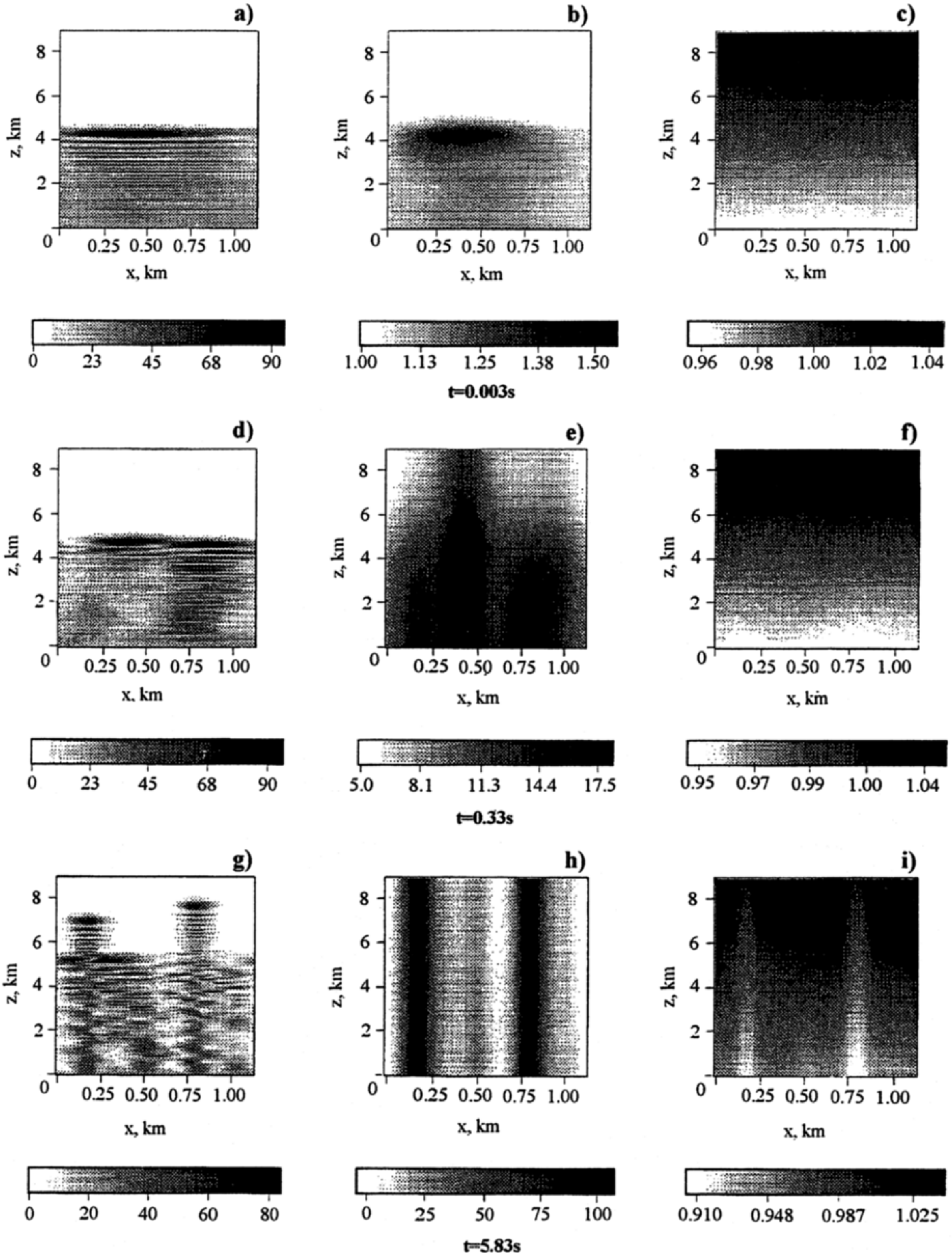

Fig. 1. Contours of the normalized wave amplitude (a, d, g), perturbed electron temperature (b; e, h) and density (c, f, i) at the time 0.003, 0.33 and 5.83 s, respectively.

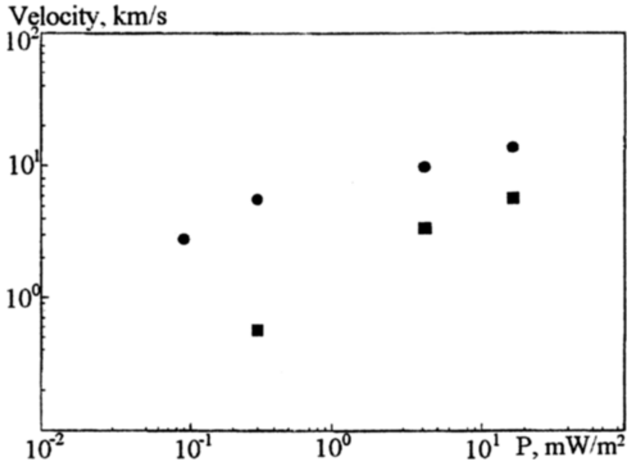

Fig. 2. Velocity of downward propagation of the temperature irregularity (solid squares) and upward propagation of the reflection height (solid circles) versus power density P.

secondary *convective* instability seeded by the irregularities spreading from the reflection height (Fig. 1d–1f). In an earlier work [34], we had shown that pre-existing density irregularities can facilitate the underdense convective instability. In our present study the seeding density irregularity arises naturally from the critical surface. Furthermore the diffusion of the heat into the overdense plasma reduces the local density in the overdense region thereby allowing the heater to propagate to heights beyond the original critical surface. This is clearly seen in Fig. 1d, where the critical surface is about 1/2 km above that in Fig. 1a.

At much later time, $t = 5.83$ s, the filaments have extended along the z direction and the transverse size of the filament has now reached a steady state. The heater wave has penetrated into the overdense region within the filaments (Fig. 1g) and since the magnitude of the heating within the filaments has increased the local temperature to a maximum of about 18% (Fig. 1h), the associated density depletions in the filaments is about a few percent as seen in the density plot (Fig. 1i) at the final time 5.83 s. We stop our simulations at this time since the wave has penetrated all the way to the top of our simulation box. The wave still has the characteristic Airy structure near the new constantly evolving reflection height, but appears to be more diffuse in the underdense region. What is interesting to observe is that even within the filaments, the density still has a weak gradient along the z direction in this quasi-stationary state.

As noted earlier, both the density and the temperature perturbations originate at the critical surface, and then diffuse both into the overdense as well as the underdense plasma. Shown in Fig. 2 is the effective velocity of propagation of the temperature irregularity (solid squares) into the underdense and the propagation of the reflection height (solid circles) into the overdense plasma, respectively, as a function of the heater power-density. These velocities were computed by dividing the distance between the original critical surface and the bottom and top boundaries respectively by the time taken to reach the boundaries. Figure 2 shows that the velocity of propagation increases with the radiated power both for upward as well as the downward propagation. The downward propagation of the thermal irregularity is faster than the upward propagation of the reflection height, but the difference diminishes as the power density of the heater increases. This can be understood qualitatively as follows. In the underdense region, the overall heating of the plasma by the radio wave as well as the lower density makes the parallel thermal conduction larger than that in the overdense plasma. This facilitates the faster propagation of the irregularity into the underdense compared to the overdense plasma. We have recently investigated the development of irregularities for 0.1 $\mathrm{mW/m^2}$. At lower power-densities the time scale for getting to quasi-steady states is very long (more than a minute). However, the spreading of the irregularity into the underdense occurs on a much shorter time scale. Based

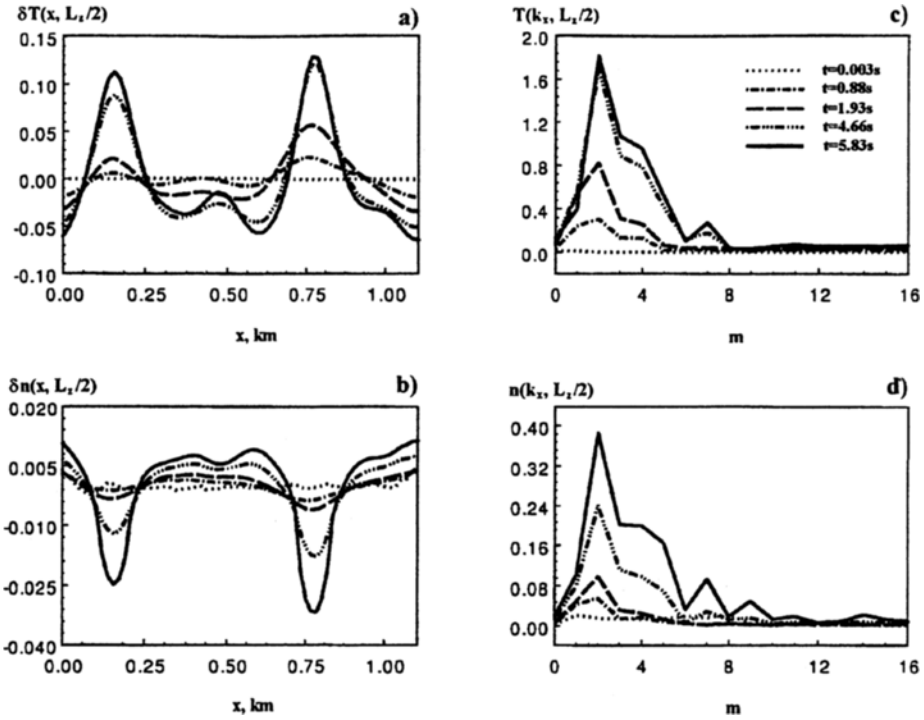

Fig. 3. Temperature (a) and density (b) fluctuations versus x, and the Fourier transform of the temperature (c) and density (d) fluctuations versus mode-number m at $z = L_z/2$ at the instants of time t =0.003, 0.88, 1.93, 4.66, and 5.83 s.

on these preliminary studies, we have found the expansion velocity into the underdense plasma for the heater power-density 0.1 mW/m^2 to be 2.5 km/s. Using backscatter radar, Bakhmet'eva et al. [35] measured the velocity of the spreading of the heater induced irregularity into the underdense plasma along the fieldline to be 2 km/s for the effective radiated power (ERP) of 70 MW. The estimated power-density for this ERP is about 0.1 mW/m^2. This is in good agreement with our result.

In Fig. 3a and 3b we show the temperature fluctuation $\delta T(x,z) = T(x,z) - \langle T(x,z)\rangle_x$ and density fluctuation $\delta n(x,z) = n(x,z) - \langle n(x,z)\rangle_x$ as a function of x, respectively, at $z = L_z/2$. The angular brackets with subscript x denotes averaging over the x direction. The Fourier spectrum of the temperature and the density fluctuation, transverse to the magnetic field at $z = L_z/2$, is plotted as a function of the mode number m in Fig. 3c and 3d, respectively. The mode number m is related to the wave number through the relationship $k_x = 2\pi m/L_x$, where L_x is the size of the computation box in the x direction. In these figures, the different curves correspond to time instants 0.003, 0.89, 1.93, 4.66 and 5.83 s, respectively. Even though the long wavelengths grow first in the early phase, the short wavelengths increase rapidly. Also evident is that the density lags behind the temperature and the spectra of the density and temperature are not identical. The density gets depleted in the region where the plasma gets preferentially heated; however, the evolution of the m spectra shows marked differences. At late time the temperature is almost in steady state while the density spectra is still evolving and the shorter wavelengths evolve as fast or faster than the long wavelength modes.

We define the normalized average temperature and density fluctuations as

$$\frac{\Delta T}{T} = \frac{\sqrt{\langle[\delta T(x,z)]^2\rangle_x}}{\langle T(x,z)\rangle_x} \tag{5}$$

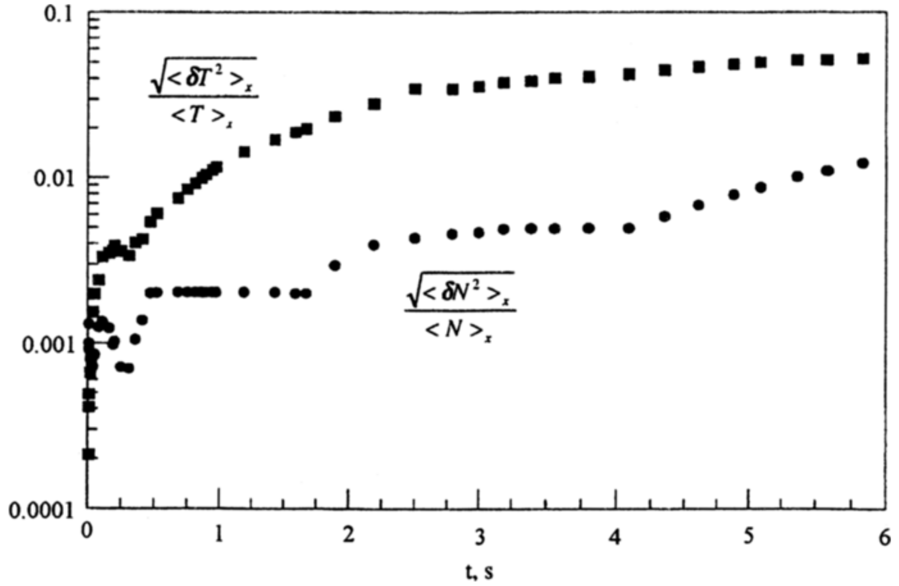

Fig. 4. Normalized average temperature fluctuation (squares) and normalized average density fluctuation (circles) at $z = 2L_z/5$ versus time.

and

$$\frac{\Delta n}{n} = \frac{\sqrt{\langle[\delta n(x,z)]^2\rangle_x}}{\langle n(x,z)\rangle_x}. \tag{6}$$

In Fig. 4, we show the time evolution of the average normalized temperature fluctuation and average normalized density fluctuation as a function of time. At very early time ($t \leq 0.1$ s) the amplitude of the average temperature and density fluctuations grow very rapidly. This is followed by a slow rise over a period of a few seconds to the saturated values. The temperature fluctuations are of the order of $5 - 10\%$, while the density fluctuations are of the order of $1 - 2\%$.

In Fig. 5 we show the wave amplitude (Figs. 5a, 5d, and 5g), temperature (Figs. 5b, 5e, and 5h) and density (Figs. 5c, 5f, and 5i) contours for power-densities P equal to 0.3 mW/m^2, 4.12 mW/m^2, and 16.46 mW/m^2, respectively. Each of these simulations was run till the wave reaches the top boundary. It took about six seconds for the wave to reach the top for $P = 0.3$ mW/m^2, one second for $P = 4.12$ mW/m^2, and half a second for $P = 16.46$ mW/m^2. The number of filaments increases as the power density increases, while their size decreases. Also, since the size of our computation box is kept the same for all three cases, the average distance between the filaments also decreases with the increase in power.

One of the important questions to address is the scaling of the transverse characteristic scalelength with the heater power. We define the correlation function $C(x, z)$ as

$$C(x,z) = \int_0^{L_x} \delta T(x + x', z)\delta T(x,z)\mathrm{d}x'. \tag{7}$$

The correlation length L_c is the distance in x for which the correlation function has decreased to $1/e$ of its peak value. In Fig. 6 we show the change in the correlation length, at $z = 2L_z/5$, for the temperature as a function of power. As the power is increased, the correlation length decreases as expected. In fact we

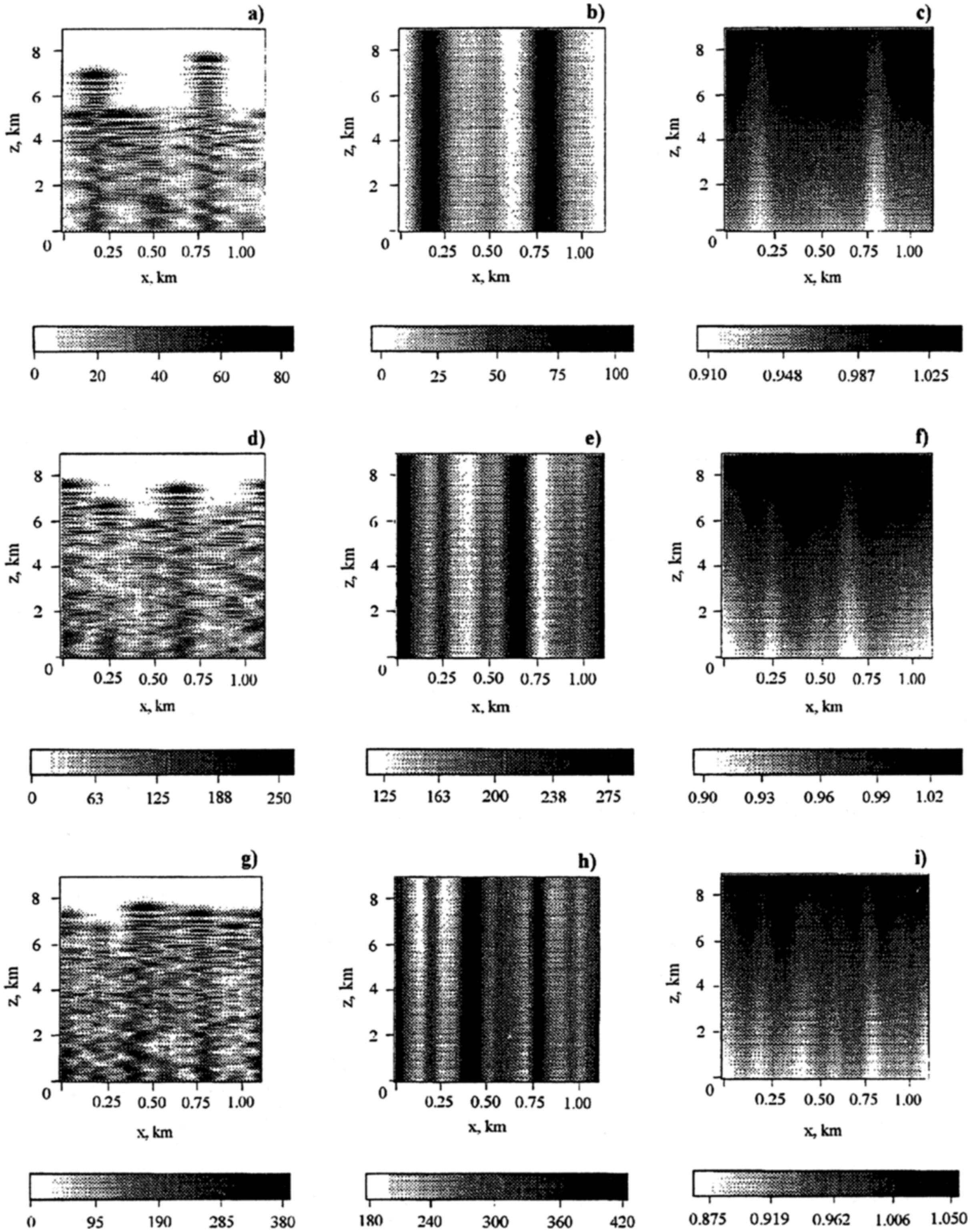

Fig. 5. Contours of the normalized wave amplitude (a, d, g) and perturbed electron temperature (b, e, h) and density (c, f, i) for power-density P equal to 0.3 mW/m^2, 4.12 mW/m^2, and 16.46 mW/m^2.

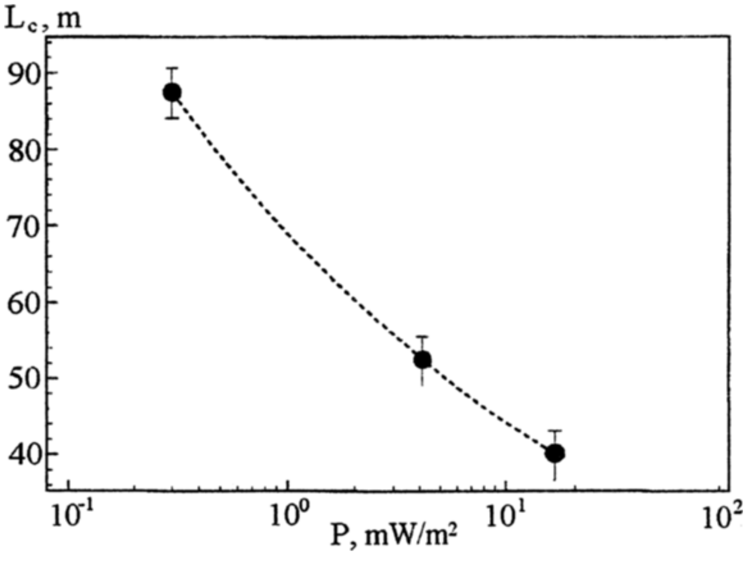

Fig. 6. Transverse correlation length L_c versus power-density P.

have found that for very high power densities (beyond the range plotted) the correlation length saturates at about 40 m. This is because the diffraction effect associated with the radio wave prevents further collapse. As discussed in our earlier work [31], the smallest scale sizes that one can expect is of the order of the electron skin-depth (where the plasma frequency ω_{p0} is evaluated at the matching height)

$$\Delta x = \frac{c}{\omega_{\mathrm{p0}}}\sqrt{\frac{n_0}{\delta n}}. \tag{8}$$

The density perturbation δn is determined by the temperature perturbation which is controlled by the parallel thermal conduction loss and the collisional loss to the background ions. For the extreme case of complete depletion of the density in the filament, the shortest transverse scale-length is electron skin-depth.

5. DISCUSSION

We have investigated the full nonlinear 2D development of the thermal self-focusing instability in the high-latitude F region ionosphere near the critical surface. The present work is an improved modelling of the density evolution compared to our earlier work [31] as well as more detailed quantification of the spatio-temporal development of the heater induced irregularities. We find that an absolute instability develops at this surface. The local heating in the vicinity of the critical surface leads to density depletion, which then spreads along the field lines. The thermal diffusion process allows for the heat to be transported into the overdense plasma. The reduction in the local density there leads to propagation of the waves and causes the field-aligned irregularity to extend into the overdense region. As the instability develops, the structures collapse in the direction transverse to the direction of the magnetic field. We have investigated the nature of the spectrum, the levels of average density and temperature fluctuations, and the correlation length of temperature fluctuations as a function of the power-density of the heater. The smallest scale-lengths of the irregularities obtained is 40 m. The associated average amplitude of the temperature irregularities is 5 − 10%, and that for the density irregularities is typically 1 − 2%. In the recent work by Basu et al. [19] electron density irregularitities in the F region, excited by the European Incoherent Scatter (EISCAT) high-power facility and observed by scintillations of the 250 MHz satellite signals, show that the spectra are in the range of kilometers to tens of meters. The spreading of the irregularity along the field line into the underdense plasma is consistent with recent observations by Bakhmet'eva et al. [35]. Since the present study only allows the wave to propagate along the magnetic field, there is very little difference between the X mode and the O mode especially since the electron gyro-frequency is much less than the wave frequency ($\Omega_e/\omega = 0.22$). In future work we will incorporate more general geometry for the wave propagation, with the direction of propagation being at a finite angle to the magnetic field.

This work was supported by NSF under the grant No.. ATM–9713719 and by the ONR.

REFERENCES

1. A. G. Litvak, *Izv. Vyssh. Uchebn. Zaved., Radiofiz.*, **11**, 814 (1970).
2. H. C. Carlson and L. M. Duncan, *Radio Sci.*, **12**, 1001 (1977).
3. H. C. Carlson, Y. V. Wickwar, and J. P. Mantas, *J. Atmos. Terr. Phys.*, **44**, 1089 (1982).
4. P. Stubbe et al., *J. Atmos. Terr. Phys.*, **55**, 1025 (1982).
5. J. A. Fejer et al., *J. Atmos. Terr. Phys.*, **47**, 1165 (1985).
6. L. M. Erukhimov et al., *Radiophys. Quant. Electron.*, **30**, 156 (1987).
7. A. Y. Wong et al., *Phys. Rev. Lett.*, **63**, 271 (1989).
8. M. T. Rietveld, H. Kohl, H. Kopka, and P. Stubbe, *J. Atmos. Terr. Phys.*, **44**, 577 (1993).
9. F. W. Perkins and E. J. Valeo, *Phys. Rev. Lett.*, **32**, 1234 (1974).
10. B. L. Cragin, J. A. Fejer, and E. Leer, *Radio Sci.*, **12**, 273 (1977).
11. A. V. Gurevich, *Nonlinear Phenomena in the Ionosphere*, Springer-Verlag, New York (1978).
12. F. W. Perkins and M. V. Goldman, *J. Geophys. Res.*, **86**, 600 (1981).
13. P. A. Bernhardt and L. M. Duncan, *J. Atmos. Terr. Phys.*, **44**, 1061 (1982).
14. P. A. Bernhardt and L. M. Duncan, *J. Atmos. Terr. Phys.*, **49**, 1107 (1987).
15. W. F. Utlaut, *J. Geophys. Res.*, **75**, 6402 (1970).
16. G. D. Thome and F. W. Perkins, *Phys. Rev. Lett.*, **32**, 1238 (1974).
17. S. Basu, S. Basu, S. Ganguli, and W. E. Gordon, *J. Geophys. Res.*, **88**, 9217 (1983).
18. S. Basu, S. Basu, P. Stubbe, H. Kopka, and J. Waaramaa, *J. Geophys. Res.*, **92**, No. 11, 149 (1987).
19. S. Basu, E. Costa, R. C. Livingston, K. M. Groves, H. C. Carlson, P. K. Chaturvedi, and P. Stubbe, *J. Geophys. Res.*, **102** (1997).
20. L. M. Duncan and R. A. Behnke, *Phys. Rev. Lett.*, **41**, 998 (1978).
21. A. Frey, P. Stubbe, and H. Kopka, *Geophys. Res. Lett.*, **11**, 523 (1984).
22. D. T. Farley, C. LaHoz, and B. G. Fejer, *J. Geophys. Res.*, **88**, 2093 (1983).
23. P. A. Bernhardt, L. M. Duncan, and C. A. Tepley, *Science*, **242**, 1022 (1988).
24. J. W. Wright, H. Kopka, and P. Stubbe, *Geophys. Res. Lett.*, **15**, 1531 (1988).
25. M. C. Kelley et al., *J. Geophys. Res.*, **100**, 17367 (1995).
26. D. F. DuBois, A. Rose Harvey, and D. Russel, *J. Geophys. Res.*, **95**, No. 21, 221 (1990).
27. J. A. Fejer, *Rev. Geophys.*, **17**, 8693 (1979).
28. P. Stubbe, H. Kopka, B. Thidé, and H. Derblom, *J. Geophys. Res.*, **89**, 7523 (1984).
29. A. C. Das and J. A. Fejer, *J. Geophys. Res.*, **84**, 6701 (1979).
30. A. V. Gurevich, A. V. Lukyanov, and K. P. Zybin, *Phys. Lett. A*, **211**, 363 (1996).

31. P. N. Guzdar, P. K. Chaturvedi, K. Papadopolous, and S. L. Ossakow, *J. Geophys. Res.*, **103**, 2231 (1998).

32. G. M. Milikh, M. J. Freeman, and L. M. Duncan, *Radio Sci.*, **29**, 1355 (1994).

33. V. L. Ginzburg, *The Propagation of Electromagnetic Waves in Plasmas, 2nd ed.*, Pergamon, New York (1970).

34. P. N. Guzdar, P. K. Chaturvedi, K. Papadopolous, M. Keskenin, and S. L. Ossakow, *J. Geophys. Res.*, **101**, 2453 (1996).

35. N. V. Bakhmet'eva, V. N. Bubukina, Yu. A. Ignat'et, et al., *J. Atm. Solar Terr. Phys.*, **59**, 2257 (1997).